frontiers | Frontiers in Earth Science

TYPE Original Research
PUBLISHED 14 April 2025
DOI 10.3389/feart.2025.1501651

OPEN ACCESS

EDITED BY
Guochang Wang,
Saint Francis University, United States

REVIEWED BY
Wei Wang,
China University of Geosciences
Wuhan, China
Wenbin Jia,
Chinese Academy of Geologi-cal Sciences
(CAGS), China
Sameer Ranjan,
Indian Institute of Technology Bombay, India

*CORRESPONDENCE
Xu Rongke,
xurongke1968@126.com

RECEIVED 25 September 2024
ACCEPTED 24 March 2025
PUBLISHED 14 April 2025

CITATION
Lin D, Xu R, Chen X, Cai P, Zheng S, Yu J, Liu J, Du W, Wang M and Xu X (2025) Sm-Nd isochron age of the calcite from shewushan carlin-type gold deposit in the middle-lower yangtze metallogenic belt, eastern China. *Front. Earth Sci.* 13:1501651.
doi: 10.3389/feart.2025.1501651

Sm-Nd isochron age of the calcite from shewushan carlin-type gold deposit in the middle-lower yangtze metallogenic belt, eastern China

Dongyong Lin[1], Rongke Xu[1]*, Xin Chen[2], Pengjie Cai[3], Shunli Zheng[2], Junzhen Yu[2], Jia Liu[4], Wenyang Du[4], Minfang Wang[2] and Xingying Xu[5]

[1]Institute of Geological Survey, China University of Geosciences, Wuhan, China, [2]The Faculty of Earth Resources, China University of Geosciences, Wuhan, China, [3]School of Earth Sciences and Engineering, Nanjing University, Nanjing, China, [4]Institute of Geological Survey, Wuhan, Hubei, China, [5]Tianjin Center of Geological Survey, China Geological Survey, Tianjin, China

The Shewushan gold deposit, situated in the western extension of Edongnan, marks the westernmost point of the Middle-Lower Yangtze Metallogenic Belt, is an important iron and copper mineralization area in the Middle-Lower Yangtze Metallogenic Belt (MLYB). Previous studies identified the Shewushan gold deposit as a Carlin-type gold ore, but its age remains controversial. This paper examines a set of widely distributed calcite veins in the Shewushan gold deposit. In hydrothermally altered carbonate rocks, calcite is texturally associated with ore-stage jasperoid and disseminated Au-bearing arsenian pyrite, suggesting synmineralization. Calcite veins concurrent with As- and Sb-sulfide mineralization are relatively enriched in middle rare earth elements and heavy rare earth elements. They yield Sm-Nd isochron age of 99.1 ± 2.4 Ma, with similar initial ε_{Nd} values, ranging from −12.2 to −12.6. These ages are interpreted to record the age of decarbonation and gold deposition of the Carlin-type gold deposits in the MLYB, formed during the late stages of the Yanshanian Orogeny. This interpretation matches the Cretaceous Sporo-pollen fossil assemblages found in the Shewushan gold deposit in red laterite, siliceous rock, and limestone. This provides the first micropaleontological evidence showing that convecting meteoric water played an important role in mineralization. Late Cretaceous Carlin-type gold mineralization further supports the conclusion that late-stage copper-gold mineralization in the MLYB occurred more likely between ~110 and 100 Ma, rather than ~123–105 Ma. It also supports that ore-forming events in the MLYB were possibly contemporaneous with other parts of Eastern China and were also controlled by the drifting direction of the subducting Pacific plate. The tectonic and mineralization evolution during the Jurassic-cretaceous in the MLYB happened during the latest Cretaceous to early Tertiary. This indicates

that the western extended part of Edongnan is not only a promising Carlin-type gold area, but also a potential target area for Cu–Mo–Au porphyry deposits, W–Cu–Au skarn deposits, Ag–Pb–Cu bearing veins, and epithermal Ag–Au deposits.

KEYWORDS

Sm-Nd geochronology, hydrothermal calcite, decarbonation and gold deposition, carlin-type gold deposit, shewushan

1 Introduction

Carlin-type gold deposits are among the most economically important gold deposits globally, with known resources concentrated mainly in Nevada in the western United States (Muntean et al., 2011) and in the Golden Triangle of South China (Hu et al., 2017). The deposits are typically hosted in carbonates and/or calcareous siliciclastic rocks and are closely associated with extensive hydrothermal alteration dominated by decarbonation, silicification, sulfidation, and argillization (Hofstra and Cline, 2000; Cline et al., 2005). The Middle-Lower Yangtze Metallogenic Belt (MLYB) is one of the most important Cu-Au-polymetallic metallogenic belts in eastern China. The copper, gold, and iron metallogenies of the MLYB occurred in the Mesozoic. They were accompanied by intense magmatism during regional tectonic phases of transition and major adjustments from the early Yanshanian Tethys tectonics to the Paleo-Pacific tectonics for the MLYB, mainly in the compression-extension conversion phase (Zhou et al., 2008; 2011; Mao et al., 2012). The main structure pattern shifted from near EW to NE or NNE (Zhai et al., 1992; Tang et al., 1998; Zhou et al., 2008). The Mesozoic intense metallogeny of the MLYB took place from ~145 to 120 Ma producing skarn, porphyry, layered copper, iron, gold, and "porphyryite iron" deposits (Nanjing-Wuhu porphyryite iron ore group, 1978; Zhai et al., 1992; Tang et al., 1998; Pan and Dong, 1999; Sun et al., 2017; Xie et al., 2019; Wang Y. et al., 2022; Li et al., 2023; Liang et al., 2023). The Mesozoic large scale mineralization process of the MLYB can generally be divided into three stages: (1) 145–135 Ma: porphyry copper-gold deposits and high-K calc-alkaline series intrusion formed mainly in the lifted block region in a strike-slip compressive tectonic setting (Zhou et al., 2011; Ma et al., 2011; Li et al., 2018; Chen et al., 2024); (2) 135–127 Ma: porphyryite iron and shoshonitic series volcanic rock formation within the basin (e.g., LuZong; Ningwu Project Group, 1978; Zhou et al., 2011; Ma et al., 2011; Chang et al., 2012; Zhang et al., 2023); (3) 127–123 Ma: uranium-gold mineralization and "A" type granite formation in both the lifted block region and basin (Zhou et al., 2011).

Several questions about Mesozoic large scale mineralization in the MLYB remain unresolved. Firstly, What is the metallogenic time and tectonic origin mechanism of the Carlin-type gold deposits in the MLYB? Although Carlin-type gold deposits such as Shewushan and Yangxin have been identified in the western extended part of Edongnan over the last 20 years, their exact formation time and the tectonic processes behind their origin, especially in relation to the large-scale mineralization during the Yanshan period, remain unclear. Secondly, What is the nature and origin of the magmatism and mineralization in the MLYB after 120 Ma? Despite the widespread magmatism and mineralization in southeastern coastal China after 120 Ma (Li, 2000; Li et al., 2023), the MLYB was previously considered a post-metallogenic stage (Chang et al., 2012). However, recent discoveries of magmatism and porphyry copper mineralization in areas like Ningzhen (110–97 Ma) suggest a more complex mineralization history (Zeng et al., 2013; Wang et al., 2014b; Wang et al., 2022 F.; Nie et al., 2016), raising the question of whether this represents a repetition of earlier stages or a distinct magmatic process. Thirdly, What are the origins of the Cu-Au porphyry deposits in the MLYB, and what mechanisms control their formation? The genesis of Cu-Au porphyry deposits in the MLYB remains debated, with proposed mechanisms including intracontinental magmatism (Hou and Yang, 2009; Lv et al., 2014; Zhou et al., 2015) and subduction of the Paleo-Pacific Plate (Ling et al., 2009; 2011; Liu et al., 2010; Li et al., 2021; Sun et al., 2021; Yan et al., 2021; Zhang et al., 2023). Further research is needed to resolve the dominant processes responsible for these deposits.

The Shewushan gold deposit, which was initially identified as a red laterite-type gold mine, was discovered in the late 1980s, with an approximately 24 Mt reserve and an average grade of about 1.8 g/t (The Forth team of Hubei Province Geological Prospecting Bureau, 1994; 1999). The Shewushan deposit, a Carlin-type gold deposit located in the Middle-Lower Yangtze Metallogenic Belt (MLYB), represents a newly identified deposit type in the region (Figure 1). The relationship between its mineralization age and the mineralization series of MLYB porphyry and lamprophyre deposits is crucial for understanding regional metallogenic events. This has significant implications for regional exploration and prospecting. The finely disseminated gold hosted within limestone below red laterite is characteristic of a Carlin-type gold deposit. Red laterite-type gold deposits are the oxidation product of Carlin-type gold ore (Liu and Li, 1995; Liu, 1995; Li, 1998). This deposit was confirmed as a typical Carlin-type deposit by Wang et al. (2014b), who studied the fluid inclusions of the mine. Many early Paleozoic fossils, including *Brachiopoda coralline*, are present within red laterite-type gold bodies and mineralized limestone (Ding, 1992); however, Cretaceous sporopollen is also present in the same stratum (Yu, 1994), and the lack of reliable isotopic dates has led to controversy over the age and genesis of the Shewushan gold deposit (Cai et al., 2016). This study focuses on the geological characteristics of calcite related to mineralization, with the goal of determining the timing of gold mineralization in the Shewushan Carlin-type gold deposit. We measured rare earth element concentrations and the isotopic compositions of Rb-Sr, Sm- Nd in calcite to establish the mineralization age. Additionally, we investigated the coexistence of paleontological fossils from two different ages (Palaeozoic and Cretaceous) within the same stratum. Exploring its potential link to large-scale Mesozoic mineralization in the Middle-Lower Yangtze Metallogenic Belt (MLYB). The relationship between this

coexistence and plate subduction dynamics was also examined. These findings contribute to a better understanding of the regional metallogenic processes and provide valuable insights for exploration and prospecting in the region.

2 Geological setting

The surface of the Shewushan gold deposit is covered by Quaternary, with sporadic outcrops (Figures 2, 3A). The Shewushan gold deposit is located in the Gao Tie duplex anticline (Figures 2, 3A), The Gao Tie duplex anticline axis is cut by an NE–SW high-angle thrust fault, and the Shewushan gold deposit is located in the Southeastern part of the anticline; anticline axis and fault present in east-west directions (Figure 4a), which is composed of early to middle Ordovician bioclastic limestone. *Sinorthis typica* Wang, *Leptella cf. Hubeiensis* Zeng, *Sinorthis* sp., and *Tritoechia* sp are present within this limestone. A Silurian carbonaceous mudstone containing thin layers of siliceous rock including graptolites, e.g., *Orthograptus* sp., *Climacograptus* sp., and *Climacograptus cf. Antiquus lineatus* Elles and wood, overlies the Ordovician limestone. The near-horizontal, low-angle Brachiopoda shell layer of the Ordovician in the deposit, which exists in the Southeastern part of the anticline in the Shewushan gold deposit, indicates that the attitude of the Ordovician–Silurian strata in this deposit is the lower angle or subhorizontal, rather than near upright as described previously (Li and Liu, 1995; Liu, 1995; Li, 1998).

The two east-west-trending high-angle reverse faults, F2 and F4 cut the country along rock and orebodies, respectively (Figures 4A, B). Deposits are commonly elongated in east-west directions parallel to these two faults (Figure 4A), indicating a close relationship between these two faults and mineralization. F2 is close to the Gao Tie duplex anticline axis; it is composed of fault breccia, fault gouge, gold-bearing siliceous stringers (Figure 5A), and calcite concurrent either with or without As-, Sb-sulfides, such as realgar and orpiment (Figure 5B). This composition implies that there was a multi-stage fault movement. In addition, northeast-southwest-trending faults appear to postdate east-west faults (Figure 4A) and are likely related to the post-metallogenic stage.

Alteration in the Shewushan Gold Mine includes silicification, sulfidization, decarbonization, bartizantion, and fluorite alteration. In the Shewushan gold deposit, gold mineralization is closely associated with decarbonation, silicification, and sulfidation. Decarbonation and silicification of limestone are evidenced by the replacement of limestone lenses within the siliceous rock (Figure 5C), the presence of a chalcedony stickwork in uneconomic low grade mineralized surrounding rock (Figure 5D), and small relict inclusions of calcite in quartz (Figures 5C–E). In addition, the major and trace element and rare earth element (REE) geochemical data show that siliceous rocks emerged through hydrothermal genesis, formed by the transmission of mineralized fluid bearing $Si0_2$ along faults to the surface, and replacing carbonate rocks to begin deposition (Wang et al., 2014a). The Shewushan gold deposit is associated with widespread hydrothermal alteration, characterized by decarbonation, silicification, sulfidation, and argillization. These features are similar to the Carlin-type gold deposits in Nevada, USA, Guizhou, China, and Osiris (Cline et al., 2005; Su et al., 2009; Steiner and Hickey, 2023).

The Shewushan Gold Mine ore is composed of both oxidized ores (laterite) and primary ores. The gold orebody is a "Z" big lens in the horizontal projection (Figure 4A), with a length of about 3,000 m, and a width of 200–600 m. The orebody output is mainly located in a single layer or two branches at depths of 0–70 m, occasionally 120–140 m below the surface. It is horizontally located in the footwall of a bedding-parallel thrust fault juxtaposing Early Silurian-Late Ordovician grey black poor permeable carbonaceous mudstone splint. It features thin layers of argillaceous slate against Early-Middle Ordovician bioclastic limestone or shell limestone splint with thin layers of carbonaceous siliceous rock. The gold orebody fault contacts wall rock (Figures 4B, C) and is mainly composed of roof horizontal oxidized orebody (laterite) and base horizontal primary orebody. The primary orebody is generally composed of fractured bioclastic limestone, with a thickness of 0–20 m and an Au grade of approximately 0.2 g/t to 3 g/t. The oxidized orebody also has a thickness of 10–20 m, with an Au grade of approximately 2 g/t, and is composed of either laterite interbedded with siliceous rocks (Figure 4B) or porous siliceous rocks splint with clay (Figure 4C) and a little silicified limestone gravel. The oxidized orebody contacts the primary orebody with a leached surface showing unconformity. At the eastern part of the deposit, early Silurian-Late Ordovician grey black carbonaceous mudstone had been denudate and the oxidized orebody had been covered by Quaternary loess.

Minor minerals include native gold, rutile, realgar, pyrite, stibnite, orpiment, cinnabar, anatase, tungsten, galena, white iron ore, epidote, apatite, dolomite, muscovite, garnet, tourmaline, and zircon (Hong and Ye, 1998). Under a microscope, no visible gold minerals were found in oxidized ores. However, electron probe and transmission electron microscopy analyses identified extremely fine (less than 0.03 μm) sub-microscopic gold particles, believed to exist because of physical adsorption or mechanical incorporation. Most gold in goethite is present as lattice gold (Hong and Ye, 1998). Under ×10,000 magnification, a small fraction of goethite particles, showing substantial gold enrichment with a composition of Au 99.82%, Ag 0.18%, and Cu 0.11%, appeared in spherical forms approximately 0.65 μm in diameter, mixed with goethite crystals (Hong and Ye, 1998). This enrichment pattern suggests that arsenian pyrite in goethite may contain independent gold minerals. Primary ore is categorized into fractured mudstone breccia and siltstone clay breccia. Arsenopyrite and realgar in primary ore are primarily distributed in a disseminated manner, with minor vein-like concentrations. In the primary ore, the gangue minerals include kaolinite, dickite, halloysite, and water mica, with minor amounts of quartz, chalcedony, and barite. The gold-bearing minerals are primarily pyrite and limonite, with gold predominantly occurring as microscopic grains within magnetite-rich rims at the margins of pyrite (Cai et al., 2016). Additionally, calcite, orpiment, realgar, cinnabar, and stibnite are also present. Consistent with Hu (2000), arsenopyrite sulfur isotopes show a broad range of variation. Electron probe microanalyzer results indicate that gold exists in arsenopyrite (850 ppm–1,550 ppm Au) and pyrite (470 ppm–1,340 ppm Au) of Shewushan primary ore (Wang et al., 2014b). The elemental composition of gold mineralization bodies displays distinct zoning: the proximal zone is characterized by As, Hg, Sb, Ba, and Ag; the mineralized zone by Au, Mo, Zn, W, F, and Pb; and the distal zone by Ni, Co., Bi, and Cu (Ni and Liu, 1995;

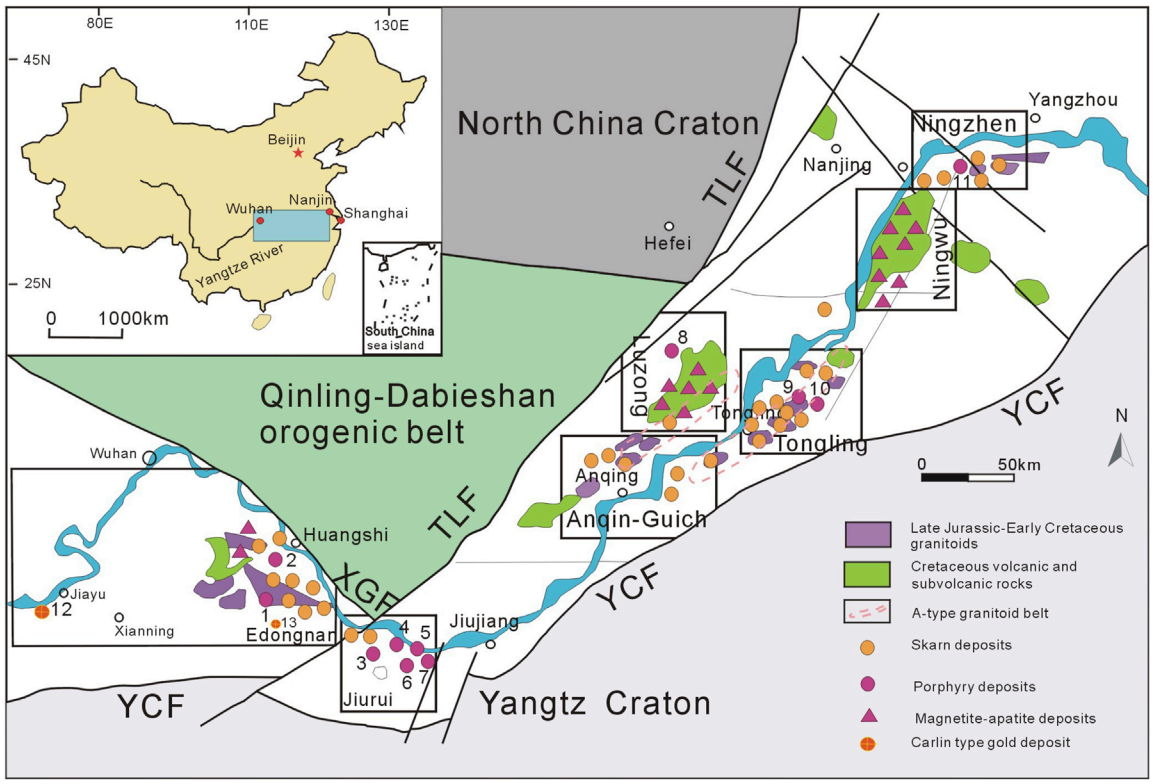

FIGURE 1
Geological map of magmatic rocks and deposits in the MLYB (modified after Zhou et al., 2015). Red circles with numbers are porphyry deposits: 1 Tongshankou Cu-Mo deposit; 2 Jiguani Cu-Au deposit; 3 Fengshandong Cu-Au deposit; 4 Wuhan Cu-Mo deposit; 5 Dingjiashan Cu deposit; 6 Yangjishan Au deposit; 7 Chengmenshan Cu-Mo deposit; 8 Shaxi Cu-Au deposit; 9 Dongguashan Cu-Au deposit; 10 Shuajiadian Cu deposit; 11 Anjishan deposit; 12 Shewushan Au deposit; 13 Fushui Au deposit.

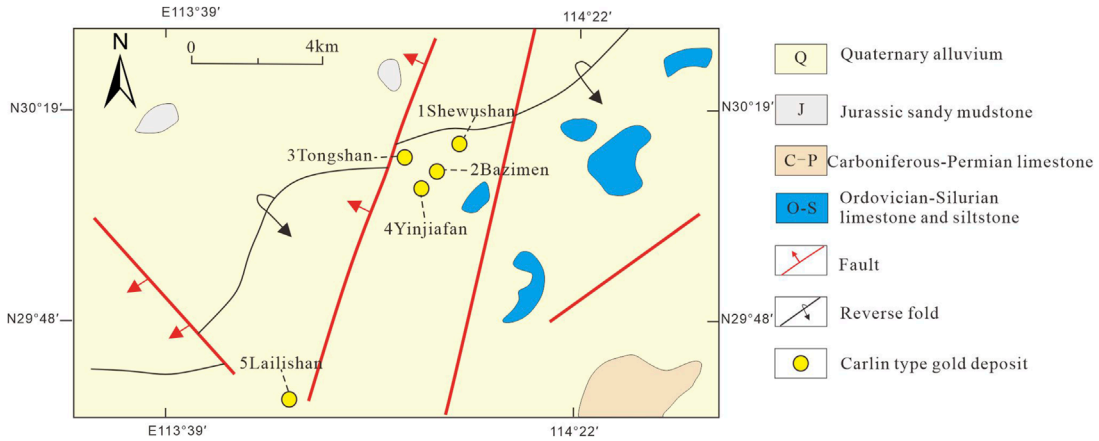

FIGURE 2
Simplified geological map (modified after Wang et al., 2014b); 1-Shewushan Au deposit; 2-Bazimen Au deposit; 3-Tangshan Au deposit; 4-Yinjiafan Au deposit; 5-lalishan Au deposit.

Li, 1998). The primary ore bodies at Shewushan occur within clastic rock or bio-clastic limestone breccia zones. Geochemical anomalies of Au-As-Sb-Hg correspond with the widespread presence of realgar, orpiment, and stibnite (Ni and Liu, 1995; Li, 1998). The sulfides in the Shewushan deposit primarily consist of gold-bearing arsenian pyrite and arsenopyrite, with smaller amounts of orpiment, realgar, and stibnite. The gold-bearing arsenian pyrite and arsenopyrite are predominantly disseminated in jasperoid quartz grains or concentrated along the grain boundaries or adjacent areas of the jasperoid quartz (Figures 3E, F; Figure 5E). The sulfur isotopic

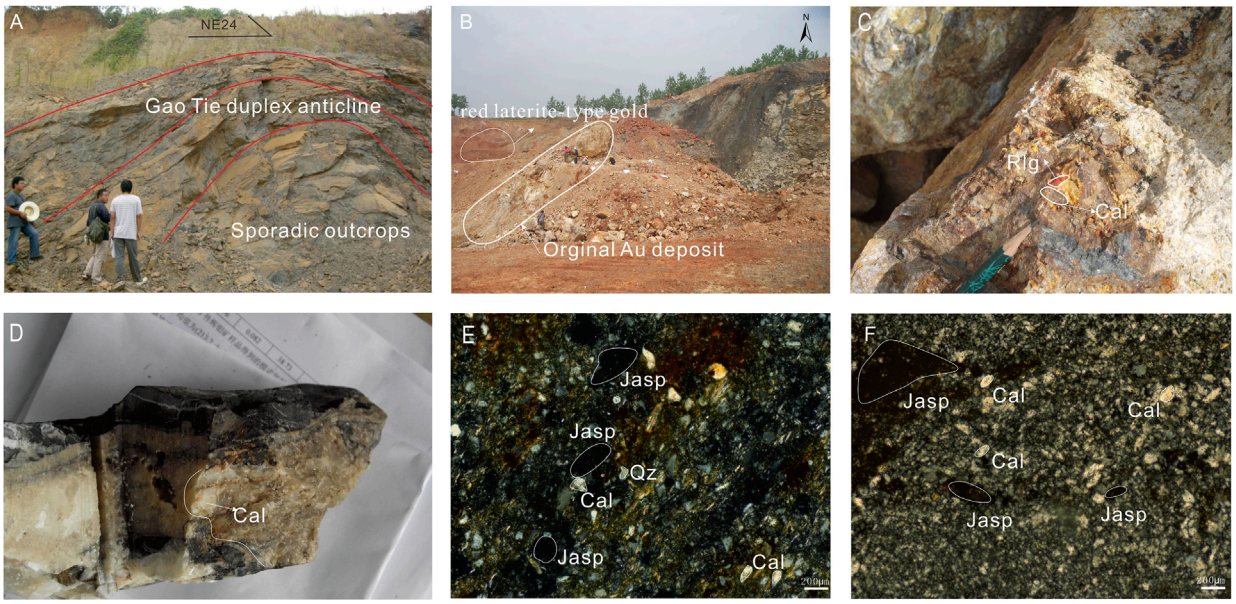

FIGURE 3
(A) Photograph of folded Silurian-Ordovician sedimentary rocks in the Gao Tie duplex anticline in the Shewushan gold deposit, **(B)** Photograph of laterite in the Shewushan gold deposit. **(C)** orpiment and/or realgar veins; **(D)** The second group of calcite veins (G2); **(E, F)** Jasperoid quartz grains or concentrated along the grain boundaries or adjacent areas of the jasperoid quartz.

values of pyrite range from −8.3‰ to +23.1‰, indicating the presence of two or more sulfur sources (Hu, 2000). In the proximal zones of carbonate dissolution, open pores and fractures are typically filled with orpiment and/or realgar veins (Figures 3C, 5F). Moving outward from these zones, calcite veins become more prevalent, often containing orpiment or realgar (Figure 5G).

Calcite veins are divided into three groups: The first group (G1) primarily fills fractures within the host rock. Veins are generally <2 cm wide, white, relatively short, have poor crystal transparency, The G1 calcite veins, which pre-mineralization, do not contain any gold or sulfides. G2 calcite veins are most likely the product of decarbonation during the main gold mineral stage. In summary, G2 is concurrent with As- and Sb-sulfide mineralizations, and features siliceous rocks fluid inclusions. Especially the spatial correlation of vein minerals to alteration zoning is assumed to have formed where acidic ore fluids were neutralized near gold mineralization, and are contemporaneous with main gold mineralization (Su et al., 2008). In this study, this spatial correlation has been used to constrain the age of gold deposition. G3 calcite veins are mostly concurrent without As- and Sb-sulfide mineralization and crosscut chalcedony veins that had formed in the main mineral stage (Figure 5E). This indicates that G3 precipitated after the main ore-stage alteration.

The second group of calcite veins (G2) commonly fill fractures or open cavities on the periphery of decarbonated rocks (Figure 3D), especially in proximity to reverse faults F2 (Figure 5B). These appear concurrent with As- and Sb-sulfides, such as realgar and orpiment (Figure 5G), occasionally stibnite and Au. G2 veins presented in large crystal clusters (Figure 5B), with weak weathering and higher transparency than G1. Two types of fluid inclusions exist in G2, namely, aqueous fluid inclusions and CO_2-rich fluid inclusions (Wang et al., 2014b). The homogenization temperatures determined from aqueous fluid inclusions in Shewushan gold deposit range from 140°C to 220°C (Wang et al., 2014b). Salinity levels range from 2.2 to 9.34 wt% NaCl eq (Liu and Li, 1995), which is consistent with Carlin-type or Carlin like-type gold deposits with an ore fluid of ~250°C and <8 wt% NaCl eq from Navada, USA (e.g., Kuehn, 1989; Hofstra et al., 1991; Lamb and Cline, 1997; Cline et al., 2005; Muntean et al., 2011). This indicates that the Shewushan gold deposit is a classical Carlin-type deposit, formed at a depth of 1.five to two km (Liu and Li, 1995; Liu, 1995; Hu, 2000; Wang et al., 2014b; Cai et al., 2016), or finely disseminated gold deposit (Li, 1998).

3 Sampling and analytical methods

The main samples of hydrothermal calcite veins concurrent with. As-, Sb-sulfides and Au,for Sm and Nd isotope dating samples were mainly obtained from along the F2 (G2: B201, HS39, BD13, BD-31,BD-13–2,F39-16),secondary sample (G2: JK230320-2,JK270320-32,JK310320-4) from the drill ZK6303. Samples from the calcite veins, collected after the main ore-stage of mineralization (G3: LS-1, G1: D112, BD102, H39-16, BD12-2, BD23, BD-28) was selected for comparison. Syn-mineralization calcite veins contain relatively higher concentrations of REEs and medium rare earth elements (MREEs) than pre-ore calcite veins, The rare earth element characteristics are similar to those observed in the Shuiyingdong and Zimudang Carlin-type gold deposits in Guizhou (Su et al., 2009; Tan et al., 2019; Wang et al., 2021); they also present variable Sm/Nd ratios suitable for isotopic dating (Bell et al., 1989; Halliday et al., 1990; Chesley et al., 1991; Darbyshire et al., 1997; Peng et al., 2003a; 2003b). The Sm-Nd isochron ages of hydrothermal calcite veins in the Shuiyindong gold deposit were successfully

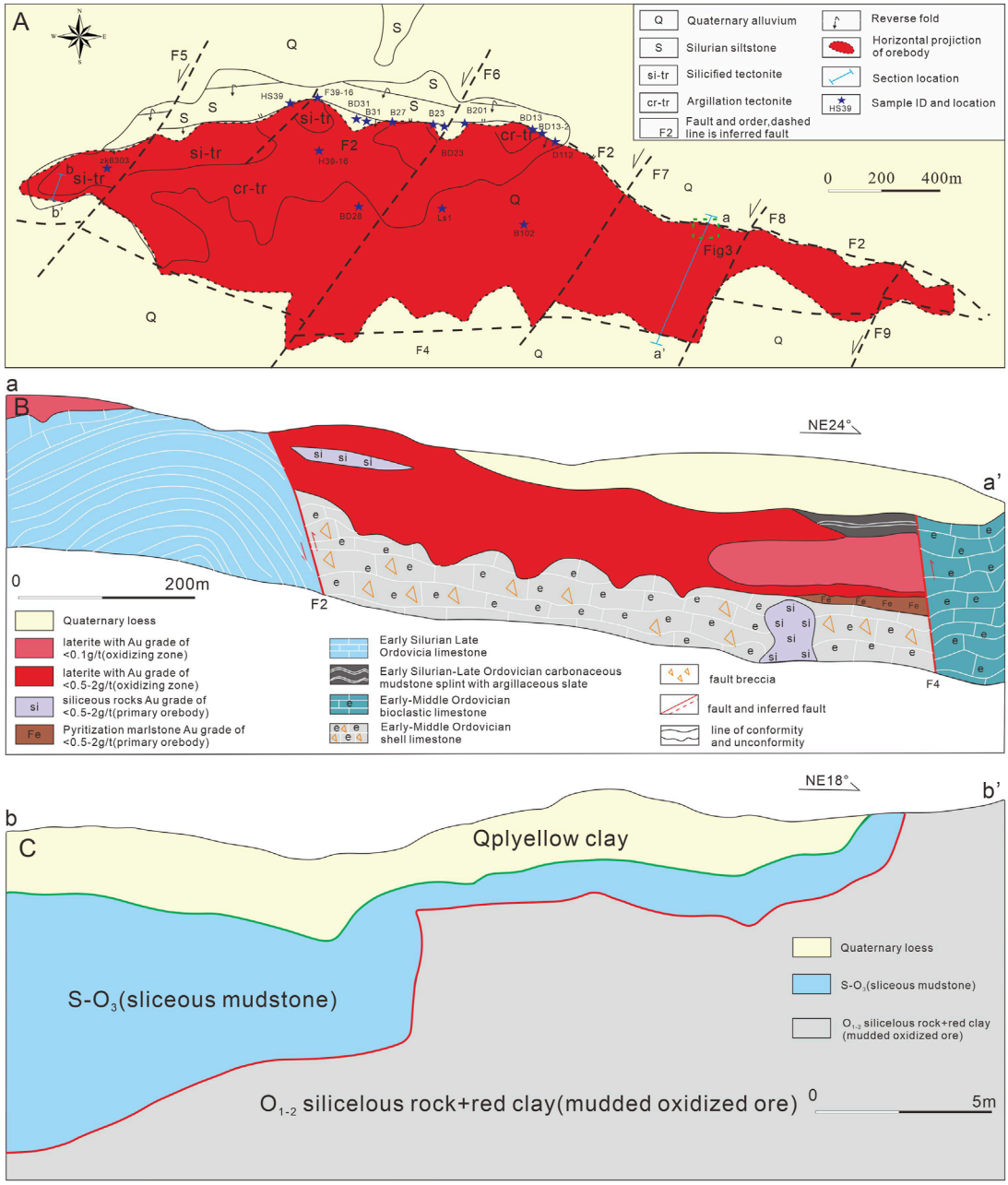

FIGURE 4
(A) Simplified geological map and the horizontal projection of the orebody in the Shewushan gold deposit (after Wang et al., 2014b); **(B)** cross section; **(C)** photograph showing the fault contact between the Early Silurian-Late Ordovician stratum and the footwall of the oxides gold orebody.

determined by Su et al. (2009). In their study, nine samples of G2 were selected to test REE, Rb-Sr, Sm-Nd, and five sample of G1 and one sample of G3 (LS-1) were selected to test REE for a comparison with G2 samples.

Pure calcite separates were hand-picked under a binocular microscope and were crushed to 200 mesh in an agate mortar. Prior to isotopic analysis, concentrations of REEs in subsamples of separated calcites were determined by inductively coupled plasma optical emission spectrometry (plasma direct-reading spectrometer JY38 S and fluorescence spectrophotometer Magix_pro2440) after acid digestion of samples in Teflon bombs at the Comprehensive rock and mineral testing Center of Wuhan, China. Sm and Nd contents and isotopic composition analyses were conducted according to procedures described by Peng et al. (2003b) and Su et al. (2009). Samples were dissolved in Teflon vessels with a mixture of HF and $HClO_4$ at a ratio of 10:1 at 150°C for at least 12 h, until decomposition was complete. Two separated sample aliquots, each weighing 150 mg, were dissolved, one for determining present-day $^{87}Sr/^{86}Sr$ and $^{143}Nd/^{144}Nd$ ratios and the other for spiking and determining Sm and Nd concentrations. Separation

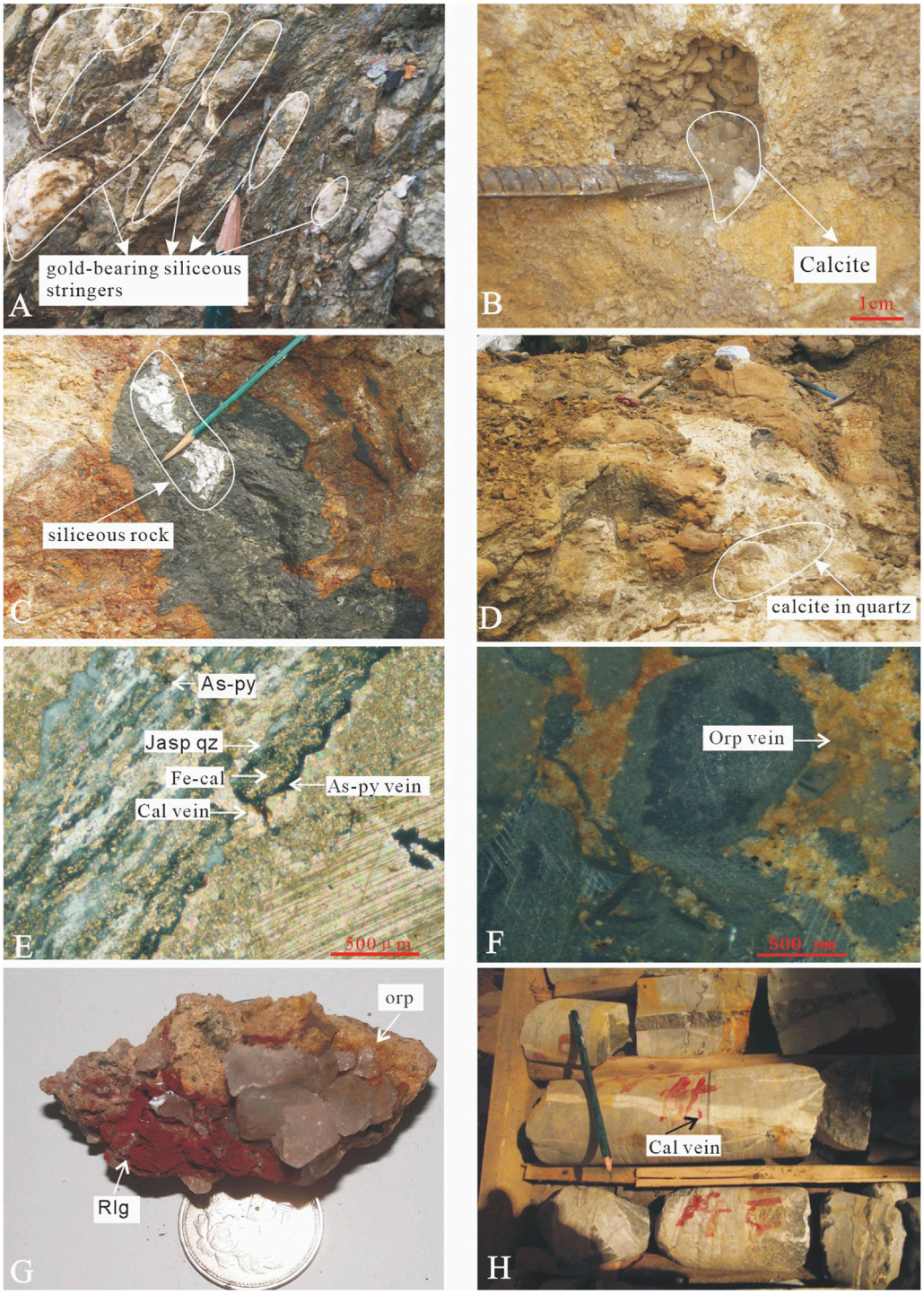

FIGURE 5
Photographs of decarbonation, silicification, sulfidation and calcite samples; **(A)** F2 composed of fault breccia and fault gouge filled with gold-bearing siliceous stringers; **(B)** calcite veins (G2) fill open cavities in proximity to reverse faults F2; **(C)** replaced residual limestone lenses in siliceous rock, the limestone lenses is intruded by arsenian pyrites string veins; **(D)** chalcedony stickwork in uneconomic low grade mineralized surrounding rock; **(E)** Photomicrograph showing relationships among jasperoid quartz, arsenian pyrite, calcite veinlets and ferroan calcite; **(F)** Photomicrograph of orpiment vein; **(G)** calcite vein concurrent with realgar and orpiment mineralization; **(H)** calcite veins filled primary gold (Au grade is about 1 ppm) 120–140 m deep in drill hole ZK6303. (Jasp qz: jasperoid quartz; As-py vein: arsenian pyrite veinlet; Cal vein: calcite veinlet; Fe-cal: ferroan calcite; Orp vein: orpiment vein; Au = gold, Cal = calcite, Qz = quartz, Rlg = realgar.).

of Sm and Nd was achieved by reverse-phase extraction with a HDEHP coated in Teflon powder. Sm and Nd concentrations were determined by isotope dilution using the ^{149}Sm-^{146}Nd spike solutions. Isotopic ratio measurements were conducted on a thermal ionization mass spectrometer at the Tianjin Institute of Geology and Mineral Resources, China. Nd isotopic ratios were normalized to a ^{146}Nd/^{144}Nd ratio of 0.7219 and Sr isotopic ratios were normalized to an ^{86}Sr/^{88}Sr ratio of 0.1194. The reproducibility of isotopic ratios was about 0.005% at the two-sigma level, and the precision of the Nd and Sm concentrations at the two-sigma level was about ±0.5% of the quoted values. Concentrations of BCR-2 determined in this study were 6.61 ppm Sm and 28.13 ppm Nd. An ^{143}Nd/^{144}Nd ratio of 0.512,633 ± 10 (2σ, n = 10), consistent with the reference value (Weis et al., 2006), was also determined. The SRM987 standard yielded an ^{87}Sr/^{86}Sr value of 0.710,245 ± 0.000025 (2σ, n = 10); and the JMC Nd standard provided a ^{143}Nd/^{144}Nd value of 0.511,132 ± 0.000020 (2σ, n = 10). Over the course of this study, blanks were 30 pg for Sm, 54 pg for Nd, and 0.56 ng for Sr The Sm-Nd isochron age was calculated using the ISOPLOT 3.0 plotting program (Ludwig, 2003). In this study, the decay constant, λ, used for ^{147}Sm was 6.54 × 10^{-12} a^{-1}, and the ^{147}Sm/^{144}Nd and ^{143}Nd/^{144}Nd values from the chondritic uniform reservoir used for the εNd(t) calculations were 0.1967 and 0.512,638, respectively.

4 Results

4.1 Rare earth elements and ^{87}Sr/^{86}Sr

REE volumes and isotopic compositions differed among G1, G3, and G2 (Tables 1, 2; Figure 6). The overall REE concentrations of G1 and G3 ranged from 1.41 to 7.81 ppm, showing enrichment with light rare earth elements (LREEs), a positive Eu anomaly (δEu = 0.63–83.67), a positive Ce anomaly (mean value = 0.34), and compositions located in the sedimentary zone of the Yb/Ca-Tb/La diagram (Figure 7A). G2, simultaneously occurring with As-, Sb-sulfides, such as realgar, and occasionally with stibnite orpiment and Au, were characterized by higher ∑REEs contents (9.70–42.70 ppm) with the exception of Fs-39 (∑REEs = 3.15 ppm); they showed a weak negative Eu anomaly (δEu = 0.61–0.86) and a positive Ce anomaly (mean value = 0.92).

The ^{87}Sr/^{86}Sr ratios measured for G2 of calcite are listed in Table 2. The measured G2 Sr isotope values ranged from 0.709,539 to 0.712,661 (Table 2). The measured Sr isotope compositions of the dated calcite samples are consistent with published values for hydrothermal calcite from the Shuiyindong gold deposit (Su et al., 2009).

4.2 Sm-Nd isochron ages

Isotope dilution measurements from the nine calcite vein samples showed Sm and Nd concentrations of 0.59–8.05 ppm and 0.19–1.94 ppm, respectively. They yielded a Sm-Nd isochron age of 99.1 ± 2.4 Ma (Figure 8), with a lower MSWD of 1.4, an initial ^{143}Nd/^{144}Nd ratio of 0.511,875 ± 5, and a range of −12.2 to −12.6 (using the CHUR values 0.1967 and 0.512,638 cited in Methods). eNd(t) is thus remarkably tight.

5 Discussion

5.1 Origins of calcite and the mineralization age of shewushan

As described above, G2 veins are relatively enriched in MREEs and heavy rare earth elements (HREEs) opposed to G1 veins. This pattern is similar to fluorite veins coeval with gold and antimony mineralization in the Qinglong district (Peng et al., 2003a), as well as calcite veins coeval with gold mineralization in the Shuiyindong gold deposit in southwest China. These ore-related calcite veins were used as a vector for exploring unexposed Carlin-type gold mineralization in the Shuiyindong district (Su et al., 2009). Samples from three drill cores (JK230320-2, JK270320-32, JK310320-4), located away from the F2 structure, show a similar heavy rare earth element (HREE) curve pattern to that of calcite veins from the F2 structure, suggesting a potential genetic relationship between the two. However, the light rare earth element (LREE) enrichment patterns in these samples, with La/Yb values comparable to those of calcite from the first category, indicate a distinct difference from the F2 calcites, reflecting compositional variation. Almost all G2 samples (except for sample Fs-39) were distributed in the hydrothermal calcite area within the calcite Yb/Ca-Tb/La diagram (Figure 7A). All samples of G2 calcite veins showed a relatively large variation in La/Ho ratios, which has little relevance to the variation of the Y/Ho ratio (Figure 7B). This is similar to cogenetic hydrothermal gangue minerals from the Tannenboden and Beihilfe mines, as described by Bau and Dulski (1995), indicating that all samples of G2 calcite veins may have the same fluid source.

Goldfarb and Groves (2015) pointed out that once fluids channeled along main faults, the hydrothermal system becomes highly fluid-dominant, making a substantial exchange along the flow path unlikely. Based on examining two group samples from G2 outcrops and drilling core samples, G2 samples showed a difference in transparency and LREE patterns. The possible reason is their location at different distances from the leading edge of the hydrothermal channel, which may indicate the result of different degrees of water-rock interaction associated with the same hydrothermal fluid. We compared the G2 REE distribution curve with those of calcite from the Shuiyindong (Su et al., 2009; Tan et al., 2019) and Zimudang (Wang et al., 2021) Carlin-type gold deposits. The G2 curve closely matches the mineralization-stage REE patterns of Shuiyindong and Zimudang, falling within the mineralization zone (Figure 6A). In contrast, the G1 and G3 curves lie below this zone, showing distinct differences from the mineralization-stage REE patterns (Figure 6B).

Fluid inclusion studies of the Shewushan deposit (Wang et al., 2014b) indicate that the homogenization temperatures range from 70°C to 350°C, with a concentration between 140°C and 220°C. Thermodynamic calculations suggest that at elevated temperatures (>250°C) Eu^{2+} should be dominant over Eu^{3+}, and may substitute for Ca^{2+} preferentially over trivalent REEs in calcite, leading to positive Eu anomalies (G1). The weak Eu anomalies (G2、G3) observed in this study are in accordance with fluid inclusion studies, showing that homogenization temperatures of fluid inclusions in calcites from Shewushan are approximately 140°C–220°C.

Ce anomalies are an indicator of reducing environments. Under oxidizing conditions, Ce^{3+} is easily oxidized into Ce^{4+}, which

TABLE 1 Rare earth element data (ppm) for calcite samples from the Shewushan deposit.

Sample no.	B201	HS39	BD13	BD-31	JK230320-2	JK270320-32	JK310320-4	BD-13–2	F39-16	LS-1	D112	BD102	H39-16	BD12-2	BD23	BD-28
Paragenetic	G2									G3	G1					
Occurrence	Cc + real									Cc						
La	0.57	0.21	0.53	1.72	5.23	6.90	2.77	0.53	0.48	0.64	0.30	2.10	1.67	0.49	0.77	0.96
Ce	1.88	0.74	1.89	5.59	12.66	15.54	8.11	1.11	0.72	0.42	0.44	1.07	2.53	0.61	1.42	1.60
Pr	0.34	0.17	0.36	0.88	1.53	2.00	1.19	0.23	0.13	0.18	0.07	0.45	0.40	0.03	0.18	0.26
Nd	2.00	1.38	2.39	5.05	6.06	8.05	5.52	1.62	0.59	0.80	0.25	1.68	1.57	0.12	0.89	1.13
Sm	0.91	1.47	1.14	1.83	1.54	1.94	1.55	0.74	0.19	0.23	0.06	0.35	0.36	0.06	0.28	0.33
Eu	0.30	0.49	0.39	0.49	0.34	0.42	0.32	0.27	0.05	0.06	0.05	0.08	0.10	2.14	0.14	0.10
Gd	1.61	2.06	1.83	2.44	1.77	2.21	1.64	1.25	0.25	0.30	0.06	0.39	0.37	0.10	0.35	0.42
Tb	0.313	0.370	0.400	0.444	0.30	0.36	0.26	0.24	0.04	0.054	0.011	0.048	0.065	0.002	0.058	0.070
Dy	1.907	1.954	2.440	2.456	1.71	2.07	1.49	1.58	0.28	0.359	0.068	0.289	0.327	0.008	0.356	0.413
Ho	0.359	0.370	0.458	0.463	0.35	0.44	0.31	0.31	0.06	0.073	0.014	0.049	0.066	0.002	0.064	0.081
Er	0.96	0.95	1.23	1.29	0.98	1.18	0.82	0.85	0.16	0.20	0.04	0.13	0.16	0.01	0.18	0.20
Tm	0.139	0.132	0.177	0.216	0.14	0.18	0.12	0.12	0.02	0.030	0.006	0.014	0.025	0.005	0.027	0.029
Yb	0.815	0.782	1.103	1.498	0.99	1.22	0.81	0.73	0.15	0.186	0.030	0.083	0.146	0.103	0.154	0.178
Lu	0.116	0.105	0.167	0.230	0.16	0.20	0.13	0.11	0.02	0.028	0.003	0.013	0.027	0.042	0.025	0.027
REE	12.21	11.18	14.51	24.59	41.41	51.44	30.83	16.94	4.86	3.55	1.41	6.74	7.81	3.72	4.90	5.80
Y	10.09	9.65	12.92	10.32	7.59	8.77	5.71	7.15	1.77	2.92	0.39	1.51	1.92	0.04	2.13	2.21
Eu/Eu*	0.76	0.86	0.82	0.71	0.63	0.62	0.61	0.86	0.70	0.74	2.33	0.63	0.84	83.58	1.36	0.85
Ce/Ce*	0.98	0.86	0.97	1.05	1.04	0.97	1.04	0.74	0.67	0.29	0.70	0.25	0.71	0.82	0.87	0.74
Y/Ho	28.11	26.09	28.20	22.30	21.68	19.94	18.43	23.06	29.44	40.06	28.09	30.79	29.12	19.00	33.34	27.26

(Continued on the following page)

10.3389/feart.2025.1501651

TABLE 1 (*Continued*) Rare earth element data (ppm) for calcite samples from the Shewushan deposit.

Sample no.	B201	HS39	BD13	BD-31	JK230320-2	JK270320-32	JK310320-4	BD-13–2	F39-16	LS-1	D112	BD102	H39-16	BD12-2	BD23	BD-28
La/Ho	1.59	0.56	1.16	3.72	14.83	15.75	8.85	1.69	8.24	8.76	21.14	43.30	25.35	243.00	12.06	11.87
Yb/ca (atom ratio)	4.71E-07	4.52E-07	6.37E-07	8.66E-07	5.72E-07	7.08E-07	4.71E-07	4.22E-07	8.55E-08	1.07E-07	1.73E-08	4.80E-08	8.44E-08	5.95E-08	8.90E-08	1.03E-07
Yb/La (atom ratio)	1.14	3.02	1.67	0.70	0.15	0.14	0.24	1.10	0.25	0.23	0.08	0.03	0.07	0.17	0.16	0.15

is easily adsorbed by iron and manganese oxides, resulting in a loss of cerium. Under reducing conditions, stagnation, and anoxia in the gold deposit in modern times, Ce^{4+} was restored to Ce^{3+}, accompanying the dissolution of iron and manganese oxides. No Ce/Ce*has been recognized. Ce anomalies record reducing conditions as well as subsequent burial and diagenesis (Wright et al., 1987; Rasmussen et al., 1998).

G1 calcites show weak Ce depletions (Ce/Ce*0.25–0.87), suggestive of a reducing environment. Likewise, Ce/Ce*near 1.0 in G2 calcites indicate that mineralization may have occurred ina. weakly reducing environment. δCe anomalies from G2 calcite veins in the Shewushan gold deposit vary from 0.675 to 1.053 and mainly concentrate at 1; they reflect weak negative Ce anomaly or no Ce anomaly, indicating that mineralization occurred in a weakly reducing environment.

$^{87}Sr/^{86}Sr$ ratios from G2 samples overlap with $^{87}Sr/^{86}Sr$ ratios from G1 samples, indicating that the fluid was efficiently buffered by host limestones during migration, which is likely a common characteristic of fracture-hosted calcite veins (Su et al., 2009). $^{87}Sr/^{86}Sr$ ratios dates of calcite veins in the Shewushan gold deposit can be used to identify suitable samples for Sm-Nd geochronological studies.

Based on studies of Carlin-type deposits in Nevada, USA, as well as the Youjiang Basin and West Qinling in central China, it has been concluded that the initial stages in the mineralization of Carlin-type deposits involve movement of Au-As-Sb-Hg-S-rich, Fe-poor, and weakly acidic fluids along deep-seated faults. These fluids react with wall rocks containing numerous ferroan carbonate minerals, which leads to the dissolution of these carbonate minerals. This process is termed decarbonation, which is the principal source for iron in sulfides that deposited with gold during the main ore stage (Hofstra and Cline, 2000; Cline et al., 2005; Su et al., 2008; 2018; Liu, et al., 2015). Furthermore, the abundant Ca^{2+}, sourced from this decarbonation, supplies sufficient materials for the deposition of calcite coeval with pyrite and arsenopyrite at the main ore stage (Peng et al., 2003b; Su et al., 2008).

It has been proposed that the Fe ions released into the fluid by decarbonation react with H_2S-rich fluid containing gold complexes under low to moderate temperatures and low pressures (*cf.* Gibert et al., 1998). This results in the deposition of pyrite and arsenopyrite containing nanoparticles of gold. Moreover, dissolved Ca^{2+} released by decarbonation would precipitate as calcite coeval with pyrite and arsenopyrite, constituting pyrite-arsenopyrite-calcite veins at Shewushan (Figures 5E,G). With decreasing temperatures, more calcites were deposited with stibnite, realgar, orpiment, and fluorite during the ore stage. REEs were incorporated into calcite by substitution at Ca^{2+} structural sites. In calcite, REE diffusion is slow (Cherniak, 1998). Even during diffusive alteration, REE diffusion and chemical information in calcite are quite possibly preserved (Cherniak, 1998). If no tectonic or magmatic activity occurred after Au mineralization, the influence of later thermal alteration on hydrothermal calcite veins is likely negligible. Thus, This would tend to preserve calcite Sm-Nd isotope systematics and lend credibility to the isochron age reported here, implying that gold mineralization at Shewushan occurred at 99.1 ± 2.4 Ma. Although calcites are easily altered, yet there are now many examples of plausible calcite Sm-Nd isochrons in Mesozoic ore deposits, e.g.,: Shuiyindong Au deposit 、 Zimudang

TABLE 2 Sm, Nd, and Sr isotope compositions of calcite veins from the Shewushan deposit.

Sample no.	Groups	Sm (ppm)	Nd (ppm)	$^{147}Sm/^{144}Nd$ (atomic)	$^{143}Nd/^{144}Nd$ (2σ) (Atomic)	$^{87}Sr/^{86}Sr$ (2σ)
B201	G2	2.0691	1.2638	0.3693	0.512,119 ± 8	0.710,429 ± 12
BD13		2.0934	1.3128	0.3791	0.512,121 ± 6	0.712,661 ± 16
BD31		5.2695	2.3990	0.2752	0.512,051 ± 3	0.711,299 ± 16
F39-16		1.2968	0.3160	0.1473	0.511,975 ± 13	0.709,539 ± 9
HS39		1.1021	1.6693	0.9157	0.512,467 ± 12	0.709,891 ± 6
JK230320-2		8.1775	2.3124	0.1710	0.511,976 ± 19	0.710,417 ± 14
JK270320-32		9.6721	2.6674	0.1667	0.511,990 ± 8	0.710,434 ± 17
JK310320-4		8.1698	2.6051	0.1928	0.512,000 ± 4	0.711,902 ± 12
BD-13–2		1.7295	1.3054	0.4563	0.512,179 ± 12	0.712,126 ± 19
B201	G1	1.2638	2.0691	0.3693	0.512,119 ± 3	0.710,429 ± 12
BD102		0.0894	0.3040	0.1778	0.512,413 ± 4	0.709,547 ± 23
F39-16		0.3160	1.2968	0.1473	0.511,975 ± 6	0.709,539 ± 9
BD23		0.2600	0.6789	0.2316	0.512,260 ± 8	0.710,141 ± 16
BD-28		0.2931	0.9484	0.1869	0.512,169 ± 4	0.709,541 ± 16
LS-1	G3	0.2382	0.5599	0.2572	0.512,350 ± 11	0.712,419 ± 25

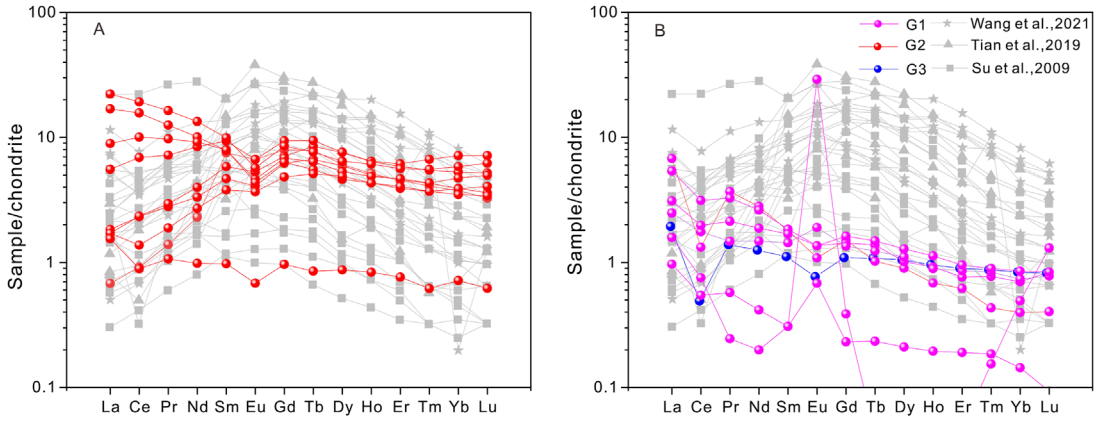

FIGURE 6
Chondrite-normalized REE patterns for calcite veins from the Shewushan deposit. All data are normalized using the chondrite REE values of Boynton, 1984; **(A)** calcite with realgar-G2; **(B)** calcite without realgar- G1, G3.

large Au deposit and Nibao gold deposit in the Youjiang Basin (Su et al., 2009; Wang et al., 2021; Ji et al., 2022). The Shewushan deposit, a Carlin-type gold deposit, shares similarities with the aforementioned deposits in terms of mineral assemblage and the relationship between gold and associated minerals. Calcite, which is commonly associated with gold in this deposit, is an ideal geochronological mineral. Thus, Sm-Nd isochrons could be used to constrain the age of the gold mineralization.

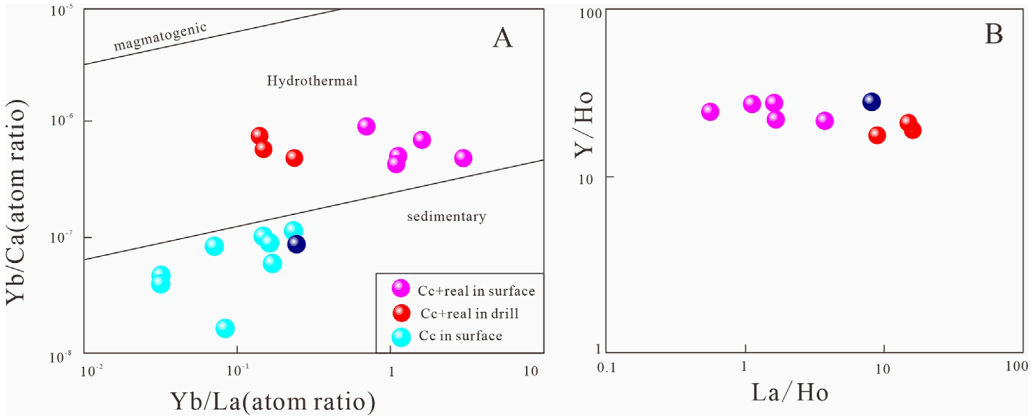

FIGURE 7
Yb/Ca-Yb/La and Y/Ho-La/Ho diagrams of calcite veins from the Shewushan deposit. **(A)** Yb/Ca-Yb/La diagram; **(B)** Y/Ho-La/Ho diagram (Bau and Dulski, 1995) (Heavy rare earth element-calcium systematics of vein calcite from Shewushan. **(A)** Yb/Ca-Yb/La diagram; **(B)** Y/Ho-La/Ho diagram) **(A)** The areas of different types of calcite are from reference (Moeller and Morteani, 1983); **(B)** diagram are from reference (Bau and Dulski, 1995).

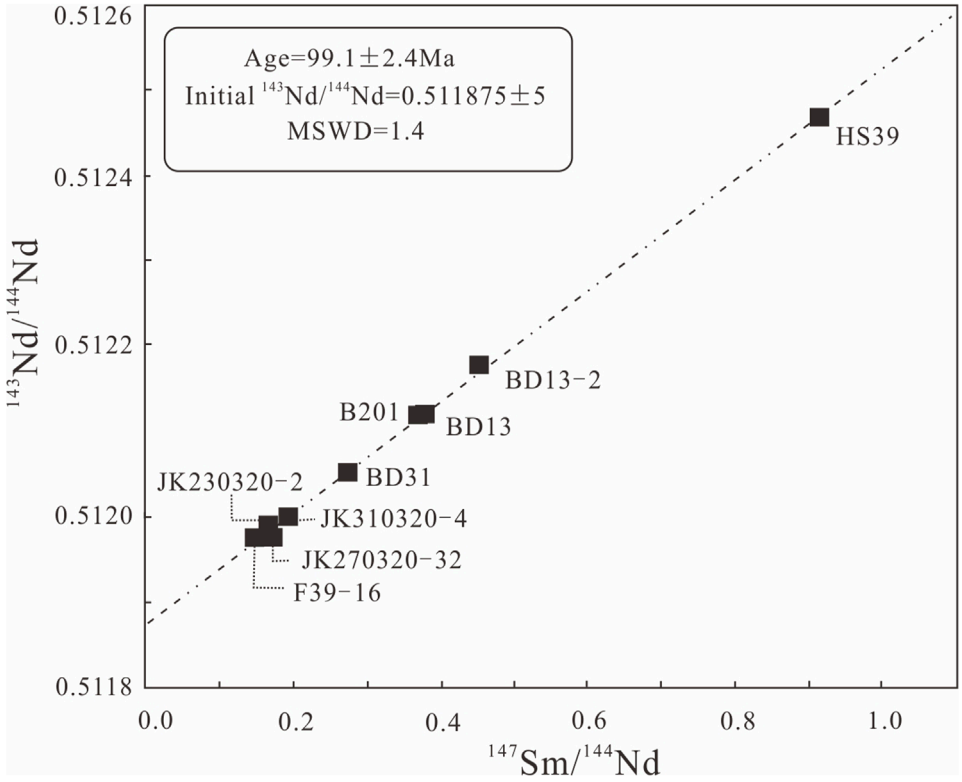

FIGURE 8
Sm-Nd isochron age for calcite veins from the Shewushan deposit.

5.2 Connection between Cretaceous Sporo-pollen fossils and mineralization

Lateritic rocks and limestones at Shewushan contain a rich microfossil flora which can be used to examine the geological and geochronological evidence. The Paleozoic fossils, *Hayasakaia* sp., *Fistulipora* sp., and *Armenoceras* were found in red laterite, siliceous rock, and limestone in the Shewushan gold deposit (Ding, 1992). Cretaceous sporo-pollen fossil assemblages have been identified within black carbonaceous shale and breccia at depths of 60–70 m below the surface in drill hole ZK004, as well as in other drill locations (Yu, 1994). These assemblages are predominantly composed of gymnosperm and fern pollen (Yu, 1994). Based on these findings, Yu (1994) proposed an analysis of the oxidation,

transportation, and re-deposition processes that occurred during the early Cretaceous. Yu (1994) argued that the red laterite-type ore deposits were the result of weathering, transportation, and re-deposition of the primary ore.

Because the formation depth of the Carlin-type ore body is 1.5–1.7 km (Liu and Li, 1995; Wang et al., 2014b), and the age of Carlin-type gold mineralization in the Shewushan gold deposit is about 100 Ma, there is no regional evidence for the uplift of 1.5–1.7 km in the early Cretaceous. And the Cretaceous Sporo-pollen fossil assemblages at black carbonaceous shale and breccia layers was attributed to weathering, transportation and re-deposition need recognizing.

Historically, genetic hypotheses for Carlin-type deposit formation comprise three general groups: circulated meteoric waters (e.g., Emsbo et al., 2003), epizonal intrusion model (Sillitoe and Bonham, 1990; Ressel et al., 2000; Heitt et al., 2003; Cunningham et al., 2004; Kelson et al., 2005), and deeply sourced ore-fluid model (Cline et al., 2005). The deeply sourced ore-fluid model involves deeply sourced magmatic and metamorphic fluids. The convection of meteoric water that derived gold from several locations in the crust was supported by δDH_2O analyses of fluid inclusions as well as alteration clay minerals from Carlin-type deposits (Hofstra et al., 1999; Hofstra and Cline, 2000; Emsbo et al., 2003; Cline et al., 2005). Enthalpy-salinity relationships and calculations in conjunction with O and H isotope data from similar Carlin-type deposits (Cline et al., 2005) indicate that incorporation of a reasonable quantity of meteoric water by vapor produces an ore fluid of ~250°C and ~two to three wt% NaCl eq., consistent with upper temperatures determined by fluid inclusions (Cline et al., 2005; Muntean et al., 2011). During the mineralization of Carlin-type deposits, the thermal energy provided by magmatism during crustal extension is the most likely energy source driving hydrothermal circulation (Henry and Boden, 1998; Hofstra et al., 1999; Muntean et al., 2011), as evidenced by the apatite fission-track anomaly in the Carlin trend (Chakurian et al., 2003; Cline et al., 2005). Also, gold from Carlin-type deposits is sourced from magma, which is supported by microanalyses of ore minerals, experimental data that describe metal partitioning, as well as age and isotopic data (Muntean et al., 2011).

Hence, Cretaceous Sporo-pollen fossil assemblages in Paleozoic shales and oxidic breccia layers in the Shewushan gold deposit may have emerged because of rising aqueous gold-bearing fluids released from magmas at depths of 10–12 km. Mixed with meteoric water, the Cretaceous Sporo-pollen fossil assemblages were carried within a few kilometers of the surface. The ~250°C and ~two to nine wt% NaCl eq mixing fluids dissolved and sulfurized the carbonate wall rocks, leading to mineralization of gold-bearing pyrite, similar to a previously suggested model (Muntean et al., 2011; Xie et al., 2017; Xie et al., 2024). The Cretaceous Sporo-pollen fossil assemblages provide unique micropaleontological evidence that the convection of meteoric water happened in Shewushan Carlin-type gold mineralization. In accordance with two or more S isotope sources and a lack of S isotope balance (Hu, 2000), according to airborne magnetic survey data, there is a hidden igneous intrusion in the east of the deposit (The Geophysical prospecting team of Hubei Province Geological Prospecting Bureau, 1992).

5.3 Time interval and feature of late-stage copper-gold mineralization in the MLYB

Previous studies showed that magmatism and associated metallogeny events after 120 Ma were widespread in China's Southeast coastal region (Chen et al., 2005; Mao et al., 2005; Zhou et al., 2007; Zhou et al., 2008); however, these are lacking in the MLYB (Chen et al., 2005; Mao et al., 2005; Zhou et al., 2007; Chang et al., 2012). It is widely accepted that the MLYB differs from another part of East China in the late Mesozoic. More recently, a series of post-120 Ma magmatic and associated metallogenic events in the MLYB, such as 106.9 ± 0.90 Ma age (SHRIMP zircon U-Pb) of Anjishan granodiorite-porphyry in Ningzhen area (Zeng et al., 2013), 109.1 ± 1.9 Ma age (SHRIMP zircon U-Pb) of Xiaoshun-Ganzi quartz diorite porphyryite, and 101.6 ± 1.1 Ma age (SHRIMP zircon U-Pb) of Shima granodiorite-porphyry (Wang et al., 2014a) have been identified. These have been ascribed to late-stage (123–105 Ma) porphyry-skarn Cu-Au mineralization. In connection with regional extension, the peak was reached, accompanied by an increase of lithospheric delamination, asthenospheric upwelling and a mantle bulge in the MLYB as reported by Zhou et al. (2015). There may be hidden igneous intrusions in the eastern portion of the deposit according to airborne magnetic survey data in the Shewushan deposit (Wang et al., 2014b). The time interval between magmatic crystallization and hydrothermal activity is 1–2 Ma (Weis et al., 2012; Karakas et al., 2017). Therefore, gold mineralization (99.1 ± 2.4 Ma) in the Shewushan deposit is the first Carlin-type gold mineralization event identified in the late stages porphyry-skarn Cu-Au mineralization in the MLYB.

The 99.1 ± 2.4 Ma Carlin-type gold mineralization in the Shewushan deposit and 97.22 ± 0.77 Ma (molybdenite Re-Os) of Donggushan tungsten polymetallic skarn deposit (Nie et al., 2016) indicate that in the MLYB, not only porphyry-skarn Cu-Au mineralization, but also Carlin-type gold mineralization and skarn W mineralization occurred in the late stages porphyry-skarn Cu-Au mineralization. Additionally, all magmatism and associated metallogeny events took place after 120 Ma in the MLYB, especially concentrated in ~110 to ~97 Ma. This range indicates that the late-stage copper-gold mineralization in the MLYB occurred more likely during 110–97 Ma, rather than 123–105 Ma, simultaneously with ~109–101 Ma voluminous high-K calc-alkaline I-type granites and A-type granitic pluton in the coastal areas of Eastern China (Li, 2000).

Throughout the years, the extent of the Paleo-Pacific subduction influence on the MLYB was debated. Certain scholars argued that the Paleo-Pacific subduction provided both the geodynamic framework and ore-forming materials for the Yanshanian MLYB magmatism and associated metallogeny (Ling et al., 2009; 2011; Liu et al., 2010; Mao et al., 2012; Xie et al., 2012; Li et al., 2014); others argued that the subduction provided only the geodynamic framework and no direct inputs of rock or ore-forming material (Wang et al., 2006a; Zhou et al., 2008; 2011; 2015; Hou and Yang, 2009; Lv et al., 2014).

Models for the Cretaceous tectonic evolution and magmatism in eastern China are a good match for the known late-Mesozoic drifting history of the Pacific plate. Especially the eastern China large-scale orogenic lode gold mineralization occurred contemporaneously with an abrupt change of ~80° in the drifting direction of the

subducting Pacific plate, which happened simultaneously with the formation of the Ontong Java Plateau (Sun et al., 2007). Surprisingly, tectonic evolution and magmatism as well as mineralization in the MLYB also mechanically matched the changes in the tectonic transport direction of the Pacific plate during the Cretaceous. During the early and middle stage (~145 Ma to ~120 Ma) copper and gold mineralization, a series of basins (e.g., Lu-Zong and Ning-Zhen) developed in the MLYB during north-south extension and rifting in the Early Cretaceous. In the late Early Cretaceous (from ~125 to 120 Ma to ~110 Ma), magmatism in the MLYB and other parts of east China generally ceased (Li, 2000). This is consistent with changes in the stress field from extension to transpression in eastern China (Zhang et al., 2003), from southward (from ~145 to ~125–122 Ma) to northwestward (at ~125–122 Ma). During the late Cretaceous (~110 Ma to ~100 Ma), magmatism and mineralization resumed in the MLYB, similar to other parts of Eastern China, which coincides with roughly east-west extension (Li, 2000; Zhang et al., 2003; Wang et al., 2005). This happened simultaneously with the turning of the drifting direction of the subducting Pacific plate by ~30°, from northwestward (from ~122 to ~110 Ma) to southwestward (at ~110–100 Ma). Magmatic events and large-scale mineralization younger than ca. 97 Ma have not yet been found in the MYLB. This age broadly coincides with northwest-southeast compressive stress and the turning of the drifting direction of the subducting Pacific plate by ~75° (Koppers et al., 2001; Sharp and Clague, 2006; Sun et al., 2007), from southwestward (from ~110 to ~100 Ma) to northwestward (at ~100 Ma). These findings further support the view advocated by Sun et al. (2007). In the Cretaceous, the major geological events in eastern China were mainly controlled by the subduction of the Pacific plate, and, in general, interactions between the plate during subduction are important driving forces for the geological evolution in eastern China and intraplate tectonics.

In this study, we discuss two key transformations in the drifting direction of the subducting Pacific plate. The first major transformation, occurring around 125–122 Ma, involved an abrupt ~80° change, which is associated with large-scale orogenic lode gold mineralization in eastern China, coinciding with the formation of the Ontong Java Plateau (Sun et al., 2007). The second transformation, characterized by a ~75° change in the plate's drift direction around 100 Ma, raises the intriguing possibility of its connection to large-scale Carlin-type gold mineralization in the MLYB.

6 Conclusion

(1) Hydrothermal calcite veins, concurrent with As- and Sb-sulfides, are relatively enriched in both MREEs and HREEs. ∑REEs contents of hydrothermal calcite veins were found to be higher than calcite veins prior to mineralization. Sm-Nd isochron ages (99.1 ± 2.4 Ma) for hydrothermal calcite veins, with initial εNd values ranging from −12.2 to −12.6, represent the age of decarbonation and gold deposition in the Shewushan gold deposit. This study provided the metallogenic age constraint of the Carlin-type gold deposit in the MLYB for the first time.

(2) The Cretaceous Sporo-pollen fossil assemblages found in red laterite, siliceous rock, and limestone are consistent with the age of decarbonation and gold deposition. This consistency provides unique micropaleontological evidence that convecting meteoric water participated in mineralization.

(3) Late-stage copper-gold mineralization in the MLYB more likely occurred from 110 to 97 Ma, rather than from 120 to 105 Ma. Age data support that ore-forming events in the MLYB were contemporaneous with other parts of Eastern China and were controlled by the tectonic transport direction of the subducting Pacific plate.

(4) The critical aspects of the tectonic history, especially the mineralogic evolution of the MLYB during the Cretaceous, resemble the Carlin-type gold deposit area of Nevada during the latest Cretaceous to early Tertiary. This similarity suggests that the west extended part of Edongnan is not only a potential Carlin-type gold area, but also a potential target area for Cu–Mo–Au porphyry, W–Cu–Au skarn deposits, Ag–Pb–Cu veins, replacement deposits, and epithermal Ag–Au deposits.

Data availability statement

The original contributions presented in the study are included in the article/supplementary material, further inquiries can be directed to the corresponding author.

Author contributions

DL: Writing – original draft. RX: Writing – review and editing. XC: Writing – review and editing. PC: Methodology, Writing – review and editing. SZ: Methodology, Writing – review and editing. JY: Software, Writing – review and editing. JL: Investigation, Writing – review and editing. WD: Methodology, Writing – review and editing. MW: Data curation, Writing – review and editing. XX: Methodology, Writing – review and editing.

Funding

The author(s) declare that financial support was received for the research and/or publication of this article. This work was supported by the Program for Cheung Kong Scholars and Innovative Research Team of the Ministry of Education (Grant No. IRT14R56), the China Geological Survey Program (Grant No. DD20160012), the Yichang Geological Exploration Fund (Grant No. YCZ2126-202301-01F), and the Project on Metallogenic Regularity of Gold Deposits in the Core of the Huangling Anticline and Target Selection for Deep-Middle Ore Prospecting in Hubei Province.

Acknowledgments

We would like to thank the Shewushan gold mining limited company and the Forth team of Hubei Province Geological Prospecting Bureau.

Conflict of interest

The authors declare that the research was conducted in the absence of any commercial or financial relationships that could be construed as a potential conflict of interest.

The reviewer WW declared a shared affiliation with the authors DL, RX, XC, SZ, JY, JL, and MW to the handling editor at time of review.

Publisher's note

References

Bau, M., and Dulski, P. (1995). Comparative study of yttrium and rare-earth element behaviours in fluorine-rich hydrothermal fluids. *Contributions Mineralogy Petrology* 119, 213–223. doi:10.1007/s004100050037

Bell, K., Anglin, C. D., and Franklin, J. M. (1989). Sm-Nd and Rb-Sr isotope systematics of scheelites:possible implications for the age and genesis of vein-hosted gold deposits. *Geology* 17 (6), 500–504. doi:10.1130/0091-7613(1989)017<0500:snarsi>2.3.co;2

Cai, P. J., Xu, R. K., Zhu, B. J., Tao, C. C., Liao, M. X., Liu, J., et al. (2016). Review and prospect of shewushan lateritic gold deposit, jiayu, Hubei province. *Geol. Rev.* 62, 389–397.

Chakurian, A. M., Arehartm, G. B., Donelick Zhang, X., and Reiners, W. P. (2003). Timing constraints of gold mineralization along the Carlin Trend utilizing apatite fission-track, 40Ar/39Ar, and apatite (U-Th)/He methods. *Econ. Geol.* 98 (6), 1159–1171. doi:10.2113/gsecongeo.98.6.1159

Chang, Y. F., Zhou, T. F., and Fan, Y. (2012). Polygenetic compound mineralization and tectonic evolution: study in the Middle-Lower Yangtze River Valley metallogenic belt. *Acta Petrol. Sin.* 28 (10), 3067–3075.

Chen, J. F., Yu, G., Yang, G., and Yang, S. H. (2005). A Geochronological framework of late Mesozoic magmatism and metallogenesis in the lower Yangtze valley,Anhui Province. *Geol. Anhui* 15 (3), 161–169.

Chen, K., Shao, Y., Liu, Z., Zhang, J., Zhang, Y., Zhan, Y., et al. (2024). Re–Os isotopes and geochemistry of pyrite from the Dongguashan Cu(-Au) deposit, Eastern China: implications for porphyry-skarn-stratabound mineralization systems. *Ore Geol. Rev.* 164, 105827. doi:10.1016/j.oregeorev.2023.105827

Cherniak, D. (1998). REE diffusion in calcite. *Earth Planet. Sci. Lett.* 160, 273–287. doi:10.1016/s0012-821x(98)00087-9

Chesley, J. T., Halliday, A. N., and Scrivener, R. C. (1991). Samarium-neodymium direct dating of fluorite mineralization. *Science* 252, 949–951. doi:10.1126/science.252.5008.949

Cline, J. S., Hofstra, A. H., Muntean, J. L., Tosdal, R. M., and Hickey, K. A. (2005). Carlin-type gold deposits in Nevada: critical geologic characteristics and viable models: *Econ. Geol. 100th Anniv.* 451–484.

Cunningham, C. G., Austin, G. W., Naeser, C. W., and Rye, R. O. (2004). Formation of a paleothermal anomaly and disseminated gold deposits associated with the Bingham Canyon porphyry Cu-Au-Mo system, Utah. *Econ. Geol.* 99, 789–806. doi:10.2113/99.4.789

Darbyshire, D. P. F., Pitfield, P. E. J., and Campbell, S. D. G. (1997). Late Archean and Early Proterozoic gold-tungsten mineralization in the Zimbabwe Archean craton: Rb-Sr and Sm-Nd isotope constraints. *Geology* 24, 19–22. doi:10.1130/0091-7613(1996)024<0019:laaepg>2.3.co;2

Ding, Q. X. (1992). Some new ideas on stratigraphy of Shewushan area. *Geol. Hubei* 5, 4–6.

Emsbo, P., Hofstra, A. H., Lauha, E. A., Griffin, G. L., and Hutchinson, R. W. (2003). Origin of high-grade gold ore, source of ore fluid components, and genesis of the Meikle and neighboring Carlin-type deposits, northern Carlin trend, Nevada. *Econ. Geol.* 98, 1069–1105. doi:10.2113/98.6.1069

Gibert, F., Pascal, M.-L., and Pichavant, M. (1998). Gold solubility and speciation in hydrothermal solutions: experimental study of the stability of hydrosulfide complex of gold (AuHS°) at 350 to 450 °C and 500 bars. *Geochmica Cosmochimica Acta* 62, 2931–2947. doi:10.1016/s0016-7037(98)00209-9

Goldfarb, R. J., and Groves, D. I. (2015). Orogenic gold: common or evolving fluid and metal sources through time. *Lithos* 233, 2–26. doi:10.1016/j.lithos.2015.07.011

Halliday, A. N., Shepherd, J. T., Dicken, A. P., and Chesley, J. T. (1990). Sm-Nd evidence for the age and origin of a MVT ore deposit. *Nature* 344, 54–56.

Heitt, D. G., Dunbar, W. W., Thompson, T. B., and Jackson, R. G. (2003). Geology and geochemistry of the Deep Star gold deposit, Carlin trend, Nevada. *Econ. Geol.* 98, 1107–1135. doi:10.2113/gsecongeo.98.6.1107

Henry, C. D., and Boden, D. R. (1998). Eocene magmatism: the heat source for Carlin-type gold deposits of northern Nevada. *Geology* 26, 1067–1070. doi:10.1130/0091-7613(1998)026<1067:emthsf>2.3.co;2

Hofstra, A. H., and Cline, J. S. (2000). Characteristics and models for carlintype gold deposits. *Rev. Eco. Geol.* 13, 163–220.

Hofstra, A. H., Leventhal, J. S., Northrop, H. R., Landis, G. P., Rye, R. O., Birak, D. J., et al. (1991). Genesis of sediment-hosted disseminated-gold deposits by fluid mixing and sulfidization: chemical-reaction-path modeling of ore-depositional processes documented in the Jerritt Canyon district, Nevada. *Geology* 19, 36–40. doi:10.1130/0091-7613(1991)019<0036:goshdg>2.3.co;2

Hofstra, A. H., Snee, L. W., Rye, R. O., Folger, H. W., Phinisey, J. D., Loranger, R. J., et al. (1999). Age constraints on Jerritt Canyon and other Carlin-type gold deposits in the western United States-relationship to mid-Tertiary extension and magmatism. *Econ. Geol.* 94, 769–802. doi:10.2113/gsecongeo.94.6.769

Hong, H. L., and Ye, X. X. (1998). Study on characteristics of the gold in the lateritic gold mine. *J. Chin. Electron Microsc. Soc.* 17 (3), 267–271.

Hou, Z. Q., and Yang, Z. M. (2009). Porphyry deposits in continental settings of China: geological characteristics, magmatic-hydrothermal system, and metallogenic model. *Acta Geol. Sin.* 83 (12), 1779–1817.

Hu, L. S. (2000). *Weathering crust structure,element geochemical behavior and geological prospecting model of the gold deposit in Hubei Shewushan.Tutor:Yao Shuzheng, Li Jiuquan*. Wuhan: China University of Ceosciences, 1–115.

Hu, R. Z., Fu, S. L., Huang, Y., Zhou, M. F., Fu, S. H., Zhao, C. H., et al. (2017). The giant South China Mesozoic low-temperature metallogenic domain: reviews and a new geodynamic model. *J. Asian Earth Sci.* 137, 9–34. doi:10.1016/j.jseaes.2016.10.016

Ji, X. Z., Bagas, L., Han, Z. H., and Liu, W. G. (2022). Sm-Nd isochron age and Sr-Nd isotopes of the calcite from the Nibao gold deposit in the Youjiang Basin, SW China. *Resour. Geol.* 72 (1), e12292. doi:10.1111/rge.12292

Karakas, O., Dufek, J., Mangan, M. T., Wright, H. M., and Bachmann, O. (2017). Thermal and petrologic constraints on lower crustal melt accumulation under the Salton Sea Geothermal Field. *Earth Planet. Sci. Lett.* 467, 10–17. doi:10.1016/j.epsl.2017.02.027

Kelson, C. R., Crowe, D. E., and Stein, H. J. (2005). Geochronology and geochemistry of the Hilltop, Lewis, and Bullion mining districts and surrounding area, Battle Mountain-Eureka trend,Nevada. In: H. N. Rhoden, R. C. Steininger, and P. G. Vikre (Eds.), *Geological society of Nevada symposium 2005, window to the world*. Reno, Nevada, 15-18, pp. 25–41.

Koppers, A. A. P., Morgan, J. P., Morgan, J. W., and Staudigel, H. (2001). Testing the fixed hotspot hypothesis using 40Ar/39Ar age progressions along seamount trails. *Earth Planet. Sci. Lett.* 185, 237–252. doi:10.1016/s0012-821x(00)00387-3

Kuehn, C. A. (1989). *Studies of disseminated gold deposits near Carlin, Nevada: evidence for a deep geologic setting of ore formation*. Middletown: Pennsylvania State University, 395.

Lamb, J. B., and Cline, J. M. (1997). Depths of formation of the meikle and betze/post deposits. Society of Economic Geologists Guidebook Series 28, pp.101–108. doi:10.5382/gb.28.07

Li, L., Lin, S., Davis, D. W., Xiao, W., Xing, G., and Yin, C. (2014). Geochronology and geochemistry of igneous rocks from the Kinging terrane: implications for Mesoarchean to Paleoproterozoic crustal evolution of the Yangtze Block. *Precambrian Res.* 255, 30–47. doi:10.1016/j.precamres.2014.09.009

Li, S. S. (1998). A further discussion on the genesis of the Shewushan lateritic gold deposit. *Min. Deposits* 17, 114–124.

Li, X. H. (2000). Cretaceous magmatism and lithospheric extension in Southeast China. *J. Asian Earth Sci.* 18, 293–305. doi:10.1016/s1367-9120(99)00060-7

Li, Y., Selby, D., Li, X., and Ottley, C. J. (2018). Multisourced metals enriched by magmatic-hydrothermal fluids in stratabound deposits of the Middle–Lower Yangtze River metallogenic belt, China. *Geology* 46 (5), 391–394. doi:10.1130/g39995.1

Li, Z., Chen, C., Chen, B., Cai, H. (2021). Early cretaceous crust–mantle interaction in the Middle-lower Yangtze River Metallogenic Belt, East China: Li–Nd–Sr

isotopic and elemental constraints. *Lithos* 398-399, 106308. doi:10.1016/j.lithos.2021.106308

Li, Z., Xia, Q., and Liu, Y. (2023). Multiple generations of garnet, zircon and titanite: temporal constraints on Fe skarn mineralization in the Middle-Lower Yangtze River Valley Metallogenic Belt, eastern China. *Lithos* 440-441, 107028. doi:10.1016/j.lithos.2023.107028

Liang, X., Wang, F. Y., Zhou, T. F., Wei, C. S., Zhang, L., Guo, X. Z., et al. (2023). Metallogenic mechanism of cobalt in the Zhuchong cobalt-rich skarn iron deposit in the Middle-Lower Yangtze River Valley Metallogenic Belt: constrained by *in-situ* sulfur isotopes and zircon U-Pb dating. *Acta Petrol. Sin.* 39 (10), 3015–3030. doi:10.18654/1000-0569/2023.10.10

Ling, M. X., Wang, F. Y., Ding, X., Hu, Y. H., Zhou, J. B., Zartman, R. E., et al. (2009). Cretaceous ridge subduction along the lower Yangtze river belt, eastern China. *Econ. Geol.* 104, 303–321. doi:10.2113/gsecongeo.104.2.303

Ling, M. X., Wang, F. Y., Ding, X., Zhou, J. B., and Sun, W. D. (2011). Different origins of adakites from the dabie mountains and the lower Yangtze river belt, eastern China: geochemical constraints. *Int. Geol. Rev.* 53, 727–740. doi:10.1080/00206814.2010.482349

Liu, J. J., Dai, H. Z., Zhai, D. G., Wang, J. P., Wang, Y. H., Yang, L. B., et al. (2015). Geological and geochemical characteristics and formation mechanisms of the Zhaishang Carlin-like type gold deposit,western Qinling Mountains, China. *Ore Geol. Rev.* 64, 273–298. doi:10.1016/j.oregeorev.2014.07.016

Liu, S. A., Li, S. G., He, Y. S., and Huang, F. (2010). Geochemical contrasts between early Cretaceous ore-bearing and ore-barren high-Mg adakites in central-eastern China: implications for petrogenesis and Cu-Au mineralization. *Geochim. Cosmochim. Acta* 74, 7160–7178. doi:10.1016/j.gca.2010.09.003

Liu, S. M., and Li, J. X. (1995). Geology and genesis of shewushan carlin-type of gold deposit in Hubei province. *J.Precious Metall.Geol* 4, 184–192.

Liu, Y. J. (1995). Some superficial opinions about the genesis of the Shewushan gold deposit. *Geol. Hubei* 9 (1), 84–90.

Ludwig, K. R. (2003). Isoplot 3.0- A geochronological toolkit for microsoft excel, 4. Berkeley Geochronology Center Special Publication, 1–70.

Lv, Q. T., Dong, S. W., Shi, D. N., Tang, J. T., Jiang, G. M., Zhang, Y. Q., et al. (2014). Lithosphere architecture and geodynamic model of middle and lower reaches of Yangtze belt: a review from SinoProbe. *Acta Petrol. Sin.* 30 (4), 889–906.

Ma, L. C., Dong, S. W., Zhong, Y. B., Zhang, Q. M., and Gao, C. S. (2011). Metallogenic epoch of the longqiao iron deposits at the lujiang-zongyang ore concentrated area in the middle and lower reaches of Yangtze river, China. *Acta Geol. Sin.* 24 (3), 193–205.

Mao, J. W., Duan, C., Liu, J. L., and Zhang, C. (2012). Metallogeny and corresponding mineral deposit model of the Cretaceous terrestrial volcanic-intrusive rocks-related polymetallic iron deposits in Middle-Lower Yangtze River Valley. *Acta Petrol. Sin.* 28 (1), 1–14.

Mao, J. W., Xie, D. Q., Li, X. F., Zhang, Z. H., Wang, Y. T., Wang, Z. L., et al. (2005). Geodynamic process and metallogeny:History and present recearch trend,with a special discussion on continental accretion and related metallogeny throughout geological history in South China. *Min. Deposits* 24 (3), 193–205.

Moeller, P., and Morteani, G. (1983). "On the geochemical fractionation of rare earth elements during the formation of Ca-minerals and its application to problems of the genesis of ore deposits," in *The significance of trace elements in solving petrogenetic problems and controversies*, 747–791.

Muntean, J. L., Cline, J. S., Simon, A. C., and Longo, A. A. (2011). Magmatichydrothermal origin of Nevada's Carlin-type gold deposits. *Nat. Geosci.* 4, 122–127. doi:10.1038/ngeo1064

Ni, J. X., and Liu, S. M. (1995). Geological features of shewushan carlin tyde of gold deposit in Hubei province. *Resour. Environ. and Eng.* (01), 91–99+90.

Nie, L. Q., Zhou, T. F., Fan, Y., Zhang, Q. M., Zhang, M., and Wang, L. H. (2016). LA-ICPMS U-Pb zircon age and molybdenite Re-Os dating of Donggushan, the first tungsten deposit found in the Luzon orefield, Middle-Lower Yangtze River Valley Metallogenic Belt. *Acta Petrol. Sin.* 32 (2), 303–318.

Ningwu Project Group (1978). *The porphyryite iron deposit of Ningwu*. Beijing: Geological Publishing House, 1–320.

Pan, Y. M., and Dong, P. (1999). The Lower Changjiang (Yangzi/Yangtze River)metallogenic belt,east central China: intrusion-and wall rock-hosted Cu-Fe-Au, Mo, Zn, Pb, Ag deposits. *Ore Geol. Rev.* 15 (4), 177–242. doi:10.1016/s0169-1368(99)00022-0

Peng, J. T., Hu, R. Z., and Burnard, P. G. (2003b). Samarium–neodymium isotope systematics of hydrothermal calcites from the Xiangshan antimony deposit (Hunan, China): the potential of calcite as a geochronometer. *Chem. Geol.* 200, 129–136. doi:10.1016/s0009-2541(03)00187-6

Peng, J. T., Hu, R. Z., and Jiang, G. H. (2003a). Samarium-neodymium isotope system of fluorites from the Qinglong antimony deposit, Guizhou Province: constraints on the mineralizing age and ore-forming minerals' sources. *Acta Petrol. Sin.* 19, 785–791.

Rasmussen, B., Buick, R., and Taylor, W. R. (1998). Removal of oceanic REE by authigenic precipitation of phosphatic minerals. *Earth Planet. Sci. Lett.* 164, 135–149. doi:10.1016/s0012-821x(98)00199-x

Ressel, M. W., Noble, D. C., Henry, C. D., and Trudel, W. S. (2000). Dike-hosted ores of the Beast deposit and the importance of Eocene magmatism in gold mineralization of the Carlin Trend, Nevada. *Econ. Geol.* 95, 1417–1444. doi:10.2113/95.7.1417

Sharp, W. D., and Clague, D. A. (2006). 50-Ma initiation of Hawaiianemperor bend records major change in Pacific plate motion. *Science* 313, 1281–1284. doi:10.1126/science.1128489

Sillitoe, R. H., and Bonham, H. F. J. (1990). Sediment-hosted gold deposits: distal products of magmatic-hydrothermal systems. *Geology* 18 (2), 157. doi:10.1130/0091-7613(1990)018<0157:shgddp>2.3.co;2

Steiner, A. P., and Hickey, K. A. (2023). Fluid partitioning between veins/fractures and the host rocks in Carlin-type Au deposits: a significant control on fluid-rock interaction and Au endowment. *Miner. Deposita* 58 (4), 797–823. doi:10.1007/s00126-022-01159-3

Su, W. C., Dong, W. D., Zhang, X. C., Shen, N. P., Hu, R. Z., Alber, t.H. H., et al. (2018). Carlin-type gold deposits in the dian-qian-gui "golden triangle" of southwest China. *Rev. Econ. Geol.* 20, 157–185.

Su, W. C., Hu, R. Z., Xia, B., Xia, Y., and Liu, Y. T. (2009). Calcite Sm-Nd isochron age of the Shuiyindong Carlin-type gold deposit,Guizhou, China. *Chem. Geol.* 258, 269–274. doi:10.1016/j.chemgeo.2008.10.030

Su, W. C., Xia, B., Zhang, H. T., Zhang, X. C., and Hu, R. Z. (2008). Visible gold in arsenian pyrite at the Shuiyindong Carlin-type gold deposit, Guizhou, China: implications for the environment and processes of ore formation. *Ore Geol. Rev.* 33, 667–679. doi:10.1016/j.oregeorev.2007.10.002

Sun, W., Yuan, F., Jowitt, S. M., Zhou, T., Hollings, P., Liu, G., et al. (2017). Geochronology and geochemistry of the Fe ore-bearing zhonggu intrusions of the ningwu basin: implications for tectonic setting and contemporaneous Cu-Au mineralization in the middle–lower yangzte metallogenic belt. *Ore Geol. Rev.* 84, 246–272. doi:10.1016/j.oregeorev.2017.01.007

Sun, W. D., Ding, X., Hu, Y. H., and Li, X. H. (2007). The golden transformation of the Cretaceous plate subduction in the west Pacific. *Earth Planet. Sci. Lett.* 262, 533–542. doi:10.1016/j.epsl.2007.08.021

Sun, Y., Ma, C., and Liu, B. (2021). Important role of magma mixing in generating the Late Cretaceous Shima intrusion along the Middle-Lower Yangtze River belt: evidence from petrology, geochemistry, and zircon U-Pb-Hf isotopes. *Lithos* 390-391, 106143. doi:10.1016/j.lithos.2021.106143

Tan, Q., Xia, Y., Xie, Z., Wang, Z., Wei, D., Zhao, Y., et al. (2019). Two hydrothermal events at the Shuiyindong carlin-type gold deposit in southwestern China: insight from Sm–Nd dating of fluorite and calcite. *Minerals* 9, 230. doi:10.3390/min9040230

Tang, Y. C., Wu, Y. C., Chu, G. Z., Xin, F. M., Tu, Y. M., Cao, F. Y., et al. (1998). *Geology of copper-gold polymetallic deposits in the along-changjiang area of anhui province*. Beijing: Geological Publishing House, 1–351.

The Forth team of Hubei Province Geological Prospecting Bureau (1994). "General geological exploration Report of the ore block between 4-13 line in Shewushan gold deposit," in *Jiayu county, Hubei province,South China*, 117.

The Forth team of Hubei Province Geological Prospecting Bureau (1999). "General geological exploration Report of the ore block between 13-71 line in Shewushan gold deposit," in *Jiayu county, Hubei province, south China*, 1–95.

The Geophysical prospecting team of Hubei Province Geological Prospecting Bureau (1992). Geophysical and chemical prospecting operational report of in Puqi-Jiayu area, Hubei province, South China

Wang, F., Guo, Y., Yan, H., Gu, H., Sun, H., and Ge, C. (2022b). Geochronology and geochemistry of the W-Mo-ore-related granitic rocks from eastern Ningzhen, lower Yangtze river belt, eastern China. *Acta Geochim.* 41 (2), 288–306. doi:10.1007/s11631-021-00501-2

Wang, M., Zheng, Y., Xu, R., Liu, Y., Xiao, F., Cheng, S., et al. (2014b). Fluid inclusion, siliceous rock geochemistry of Shewushan lateritic gold deposit, Hubei Province, eastern China: implication for the genesis of primary orebody. *Chin. J. Geochem.* 33, 65–76. doi:10.1007/s11631-014-0660-8

Wang, Q., Wyman, D. A., Xu, J. F., Zhao, Z. H., Jian, P., Xiong, X. L., et al. (2006a). Petrogenesis of Cretaceous adakitic and shoshonitic igneous rocks in the Luzon area, Anhui Province (eastern China): implications for geodynamics and Cu-Au mineralization. *Lithos* 89, 424–446. doi:10.1016/j.lithos.2005.12.010

Wang, X. L., Zeng, J. N., Ma, C. Q., Li, X. F., Wu, Y. F., and Lu, S. F. (2014a). Zircon U-Pb dating of yanshanian intrusive rocks in ningzhen district, jiangsu:the chronology evidence for a new stage of petrogenesis and metallogeny in the middle and lower reaches of Yangtze river. *Front. Earth Sci.* 21 (6), 289–301.

Wang, Y., Yang, X., Wang, C., Zhang, H., Liu, S., and Sun, C. (2022a). Comparative studies on stratabound and skarn-type deposits, Tongling region, lower Yangtze River metallogenic Belt: constraints from pyrite geochemistry. *Ore Geol. Rev.* 146, 104919. doi:10.1016/j.oregeorev.2022.104919

Wang, Y. H., Houseman, G. A., Lin, G., Guo, F., Wang, Y. J., Fan, W. M., et al. (2005). Mesozoic lithospheric deformation in the North China block: numerical simulation of evolution from orogenic belt to extensional basin system. *Tectonophysics* 405, 47–63. doi:10.1016/j.tecto.2005.05.012

Wang, Z. P., Tan, Q. P., Xia, Y., Liu, J. Z., Yang, C. F., Li, S. T., et al. (2021). Sm–Nd isochron age constraints of Au and Sb mineralization in southwestern Guizhou province, China. *Minerals* 11, 100. doi:10.3390/min11020100

Weis, D., Kieffer, B., Maerschalk, C., Barling, J., Jong, J., Williams, G. A., et al. (2006). High precision isotopic characterization of USGS reference materials by TIMS and MC-ICP-MS. *Geochem. Geophys. Geosyst* 7 (8). doi:10.1029/2006gc001283

Weis, P., Driesner, T., and Heinrich, C. A. (2012). Porphyry-copper ore shells form at stable pressure-temperature fronts within dynamic fluid plumes. *Science* 338 (6114), 1613–1616. doi:10.1126/science.1225009

Wright, J., Schrader, H., and Holser, W. T. (1987). Paleoredox variations in ancient oceans recorded by rare earth elements in fossil apatite. *Geochim. Cosmochim. Acta* 51, 631–644. doi:10.1016/0016-7037(87)90075-5

Xie, G., Mao, J., Richards, J. P., Han, Y., and Fu, B. (2019). Distal Au deposits associated with Cu-Au skarn mineralization in the fengshan area, eastern China. *Econ. Geol.* 114 (1), 127–142. doi:10.5382/econgeo.2019.4623

Xie, Z., Gopon, P., Xia, Y., Douglas, J. O., Cline, J., Liu, J., et al. (2024). Does SW China have Carlin-type gold deposits? A micro-to atomic-scale perspective. *Miner. Deposita* 59 (4), 757–772. doi:10.1007/s00126-023-01231-6

Xie, G., Mao, J., and Zhao, H. (2011). Zircon U–Pb geochronological and Hf isotopic constraints on petrogenesis of Late Mesozoic intrusions in the southeast Hubei Province, Middle–Lower Yangtze River belt (MLYRB). *Environ. Sci. Technol.* 125, 697–710. doi:10.1016/j.lithos.2011.04.001

Xie, Z., Xia, Y., Cline, J. S., Yan, B., Wang, Z., Tan, Q., et al. (2017). Comparison of the native antimony-bearing Plaiting gold deposit, Guizhou Province, China, with Carlin-type gold deposits, Nevada, USA. *Miner. Deposita* 52 (1), 69–84. doi:10.1007/s00126-016-0647-y

Yan, J., Liu, X., Wang, S., Xie, J., and Liu, J. (2021). Metallogenic type controlled by magma source and tectonic regime: Geochemical comparisons of Mesozoic magmatism between the Middle–Lower Yangtze River Belt and the Dabie Orogen, eastern China. *Ore. Geolo. Rev.* 133, 104095. doi:10.1016/j.oregeorev.2021.104095

Yu, R. Y. (1994). New understanding of the ore-bearing loose strata in the Shewushan gold mining area. *Hubei. Geolo.*, 60–66.

Zeng, J. N., Li, J. W., Chen, J. H., and Lu, J. P. (2013). SHRMP Zircon U-Pb dating of Anjishan intrusive rocks in Ningzhen district, Jiangsu, and its geological significance. *Earth Sci.* 38 (1), 57–67.

Zhai, Y. S., Yao, S. Z., and Ling, X. D. (1992). *Regularities of metallogenesis for copper (gold) deposits in the middle and lower reaches of the Yangtze river area*. Beijing: Geological Publishing House, 1–120.

Zhang, J., Sun, S., Zhang, L., Deng, J., Li, S., and Sun, W. (2023). Origin of transitional I-A-type syenite and its relationship to A-type intrusions in the luzong basin, the lower Yangtze river belt: insights from geochemistry. *Chem. Geol.* 626, 121458. doi:10.1016/j.chemgeo.2023.121458

Zhang, Y. Q., Dong, S. W., and Shi, W. (2003). Cretaceous deformation history of the middle Tan-Lu fault zone in Shandong Province, eastern China. *Tectonophysics* 363, 243–258. doi:10.1016/s0040-1951(03)00039-8

Zhou, T. F., Fan, Y., and Yuan, F. (2008). Advances on petrogenesis and metallogeny study of the mineralization belt of the Middle and Lower Reaches of the Yangtze River area. *Acta Petrol. Sin.* 24 (8), 1665–1678.

Zhou, T. F., Fan, Y., Yuan, F., Zhang, L. J., Ma, L., Qian, B., et al. (2011). Petrogenesis and metallogeny study of the volcanic basins in the middle and lower Yangtze metallogenic belt. *Acta Geol. Sin.* 85 (5), 712–730.

Zhou, T. F., Wang, S. W., Fan, Y., Yuan, F., Zhang, D. Y., and White, N. C. (2015). A review of the intracontinental porphyry deposits in the Middle-Lower Yangtze River Valley metallogenic belt, Eastern China. *Ore Geol. Rev.* 65, 433–456. doi:10.1016/j.oregeorev.2014.10.002

Zhou, T. F., Yuan, F., Yue, S. C., Liu, X. D., Zhang, X., and Fan, Y. (2007). Geochemistry and evolution of ore-forming fluids of the Yueshan Cu-Au skarn and vein-type deposits. Anhui Province. South China. *Ore Geol. Rev.* 31 (2), 279–303. doi:10.1016/j.oregeorev.2005.03.016